Sol-Gel Coatings Masonry Sealer for PFAS-Replacement Coatings that Reduces Sorptivity, Acid-Induced Degradation, and Internal Steel Corrosion in Masonry Materials

S. K. Kabani[1,2], M. Khan[1,2], F. Akande[1,2], K. E. Russell[1,3,4], C. Taylor[2], E. Mellon[5], J. Gates[5,] S. A. Curran[2,4]

[1] College of Education, Department of Psychological Health and Learning Science, University of Houston, Houston, TX 77204, USA

[2] Currans Nanotechnology Research Group (CNRG), University of Houston, Houston, TX 77204, USA

[3] School of Business and Innovation, Barton College, 800 Vance St NE, Wilson, NC 27893 USA

[4] Department of Physics, Science and Research Building 1, University of Houston, Houston, TX 77204, USA

[5] Gates International Lubricants, 18906 E Industrial Pkwy, New Caney, TX 77357, Houston TX 77204, USA

Abstract

Masonry has been in use for over 6,000 years. This building material is responsible for 70% of all construction, yet masonry degradation exists as a significant operational and occupational issue. Porous features of masonry materials make it especially susceptible to corrosion through water absorption. Currently, preventive methods use sealants and paints as protective coatings to mitigate degradation and corrosion. However, these solutions have demonstrated low durability, remain permeable under environmental stress, limiting their overall effectiveness. Several of these coatings contain per- and polyfluoroalkyl substances (PFAS), which are toxic compounds linked to environmental contamination and human health concerns. PFAS emission is correlated to industrial production and manufacturing processes and transport through several environmental pathways. As a result, sol-gel coatings have emerged as a potential alternative to PFAS-containing

coatings as they are highly durable and environmentally protective. However, solgels are notoriously susceptible to high shrinkage, limited coating thickness, and challenges in manufacturing. This study evaluates the effectiveness of a novel Sol-Gel-based Self-Cleaning Hydrophobic Nanocoating (SCHN 158), which can be mass manufactured (in tons), providing economic relief while improving durability and acid resistance in all masonry materials. SCHN 158 was compared with uncoated masonry samples and commercial coatings. Mass change analysis, acid corrosion testing, and sorptivity measurements were used to test coating performance. SCHN 158 demonstrated minimal mass loss, maintained structural integrity under acid exposure, and significantly reduced water absorption compared to untreated and commercial coating samples. These findings demonstrate potential applications in manufacturing, construction, and resource extraction fields by SCHN 158's established effectiveness in limiting water and acid penetration. This highlights its potential to enhance masonry, infrastructure durability, and metal reinforcement protection in harsh conditions such as found for reinforced rebar, pipes in fracking and irrigation pipes.

Introduction

Masonry is widely used in infrastructure but is highly susceptible to degradation when exposed to aqueous and acidic environments. The porosity of masonry facilitates the permeation of water, contributing to structural deterioration. When water is trapped in masonry pores, it can act as a conduit for freeze-thaw cycles, leading to masonry expansion and internal and external cracking. Capillary water transport weakens binding agents present in masonry, resulting in gradual masonry degradation [1]. Moreover, water infiltration can accelerate corrosion of embedded steel reinforcement due to higher oxygen levels, chemical contaminants, and localized pitting [2]. This significantly reduces the structural integrity of steel reinforcement, increasing maintenance, and safety concerns. This issue has notably affected the oil and gas industry, resulting in annual global

costs of $1.372 billion in corrosion management alone [3-4]. According to a study, the estimated cost of corrosion in the United States is $276 billion, approximately 3.1% of gross domestic product [5]. This makes corrosion one of the most significant challenges currently facing the global industry.

Figure 1. *Comparison of cleaned and treated masonry (left) and normal untreated stone (right), with the untreated stone showing a prominence of rust from metal railing leaching through the masonry.*

To mitigate these effects, hydrophobic surface treatments have been widely utilized to limit water ingress and reduce corrosion-related damage. Figure 1 shows a wall with a metal railing that has been in place for over 8 years in Sugarland, Texas. The metal railing is corroded, causing rust and flakes to leach into the masonry, which in turn accelerates the deterioration of the stonework. Coating the wall after cleaning extends the structure's life by 7 years and protects it by providing a barrier. Traditional coatings have relied heavily on fluorocarbon-based chemistries, such as per- and polyfluoroalkyl substances (PFAS), often referred to as "forever chemicals." The PFAS group consists of other chemicals used in paints and coatings, such as perfluorooctanoic acid (PFOA) and perfluorooctane sulfonate (PFOS). The PFAS family includes over 12,000 compounds, varying in carbon chain length, partially or fully saturated with fluorine, and bearing polar end groups [6].

Their stability is attributed to the strength of carbon-fluorine bonds, which confer high thermal and chemical stability, making them highly resistant to environmental degradation. The length of the carbon chain and the degree of fluorine saturation are inversely correlated with detoxification rates (i.e., the longer the carbon chain and the greater the degree of fluorine saturation, the slower the detoxification rate), as illustrated in Figure 2. PFAS compounds are also amphiphilic, characterized by a hydrophobic fluorinated tail and a hydrophilic head. Typical eight-carbon chain PFA compounds (C8 compounds), such as PFOA and PFOS, were commonly used. However, they have been banned worldwide due to their carcinogenic nature. Major chemical producers have reduced the size of chain lengths (C6-C4); however, these have proved ineffective. These structures enable aqueous transport and contribute to bioaccumulation in the bloodstream or tissues of living organisms, as well as to ubiquitous environmental dispersion through bodies of water and deposition in soil [6-7].

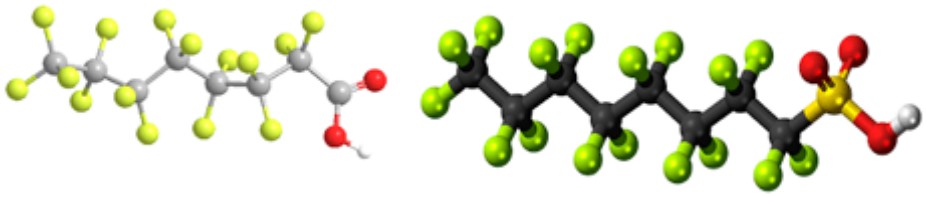

Figure 2. *Chemical structure of PFOA (perfluorooctanoic fluoride - right) and PFOS (Perfluorooctanesulfonic Acid - left) illustrating the fully fluorinated carbon backbone that contributes to hydrophobic aspects of the coating.*

While the structural features of PFAS contribute to their effectiveness as water-repellent coatings, their environmental impact includes strong bioaccumulation, with their half-lives ranging from 2 to 7 years [6]. PFAS contamination is attributed to direct and indirect emissions associated with industrial production and manufacturing processes. Primary sources include consumer goods, PFAS-containing firefighting foams, landfills, and wastewater treatment plants. Once released, PFAS can travel through multiple transport pathways, including atmospheric and

freshwater systems. These processes expedite the spread of PFAS through secondary exposure through agricultural systems and food sources, including poultry and livestock [7]. Environmental transport pathways are illustrated in Figure 3.

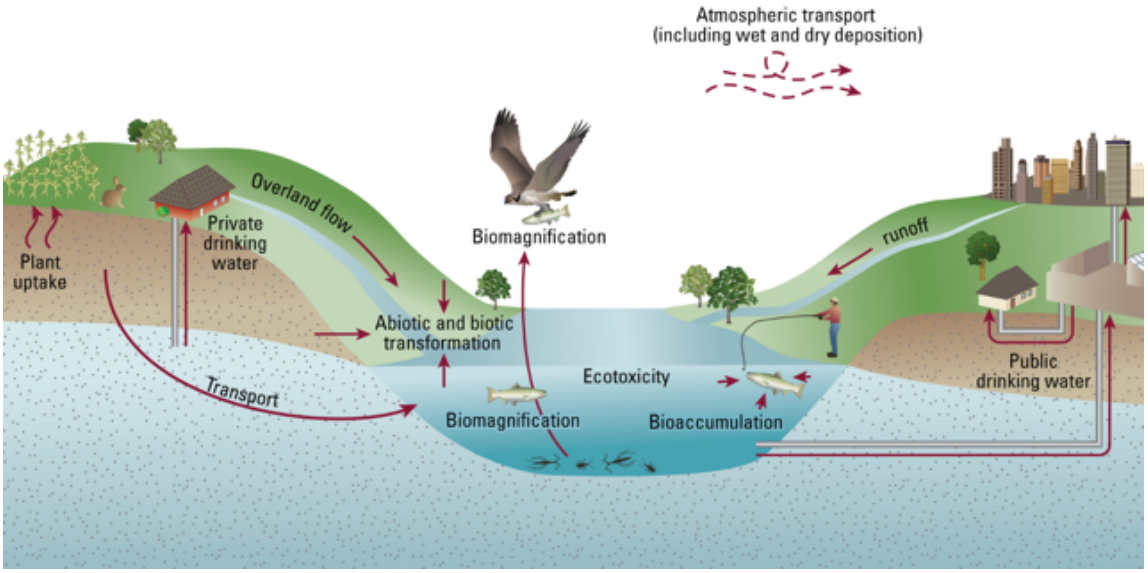

Figure 3. *Environmental fate and transport pathways of per- and polyfluoroalkyl substances (PFAS). The image illustrates the origin of PFAS from industrial emissions and primary sources, which are then transported through several environmental pathways. Illustration created by Jacqueline Olsen, USGS, public domain.*

The environmental dispersion of PFAS ultimately accumulates in final receptors such as wildlife, fish, birds, and humans. The widespread distribution of PFAS highlights its capabilities to migrate through interconnected environmental systems, advancing long-term contamination [7].

Due to their widespread exposure and resistance to degradation, PFAS persist and accumulate in the body over time, posing significant human health concerns. The Environmental Protection Agency (EPA) explains the adverse health effects caused by exposure, including reproductive issues such as decreased fertility, developmental effects in children including low birth weight and accelerated puberty, and increased risks of certain cancers such as kidney and

testicular cancer. Additionally, research states the linkage between PFAS and immune system suppression, hormonal disruption, and increased cholesterol levels [8].

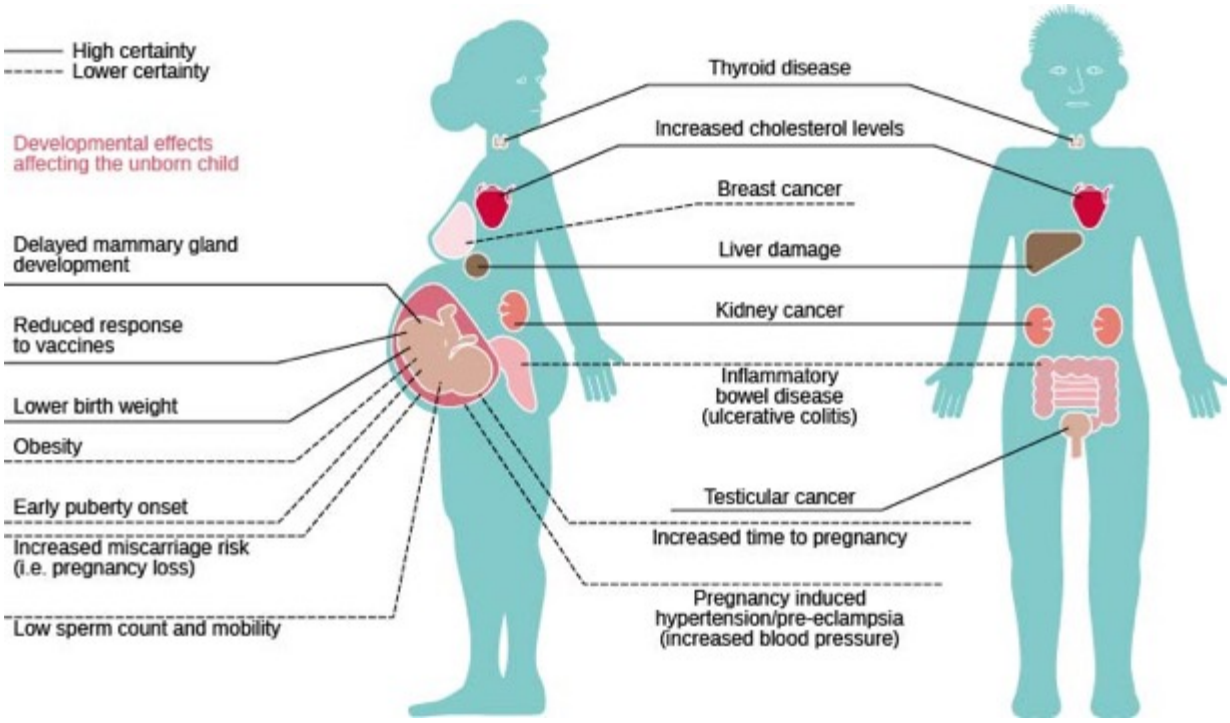

Figure 4. *Overview of health effects associated with PFAS exposure, such as cancer, hormonal disruption, immune effects, and developmental impacts. European Environment Agency (Q632988) (original image) (vectorization), CC BY 2.5 DK <https://creativecommons.org/licenses/by/2.5/dk/deed.en>, via Wikimedia Commons.*

Recent reports indicate that PFAS-containing compounds remain prevalent in commercial coating products, often without clear disclosure. A study conducted by Healthy Building Network (HBN) analyzed 94 paint samples from major manufacturers (i.e., Sherwin-Williams, Valspar, Behr) and found that 50% of the samples had detectable levels of fluorine, an indicator of PFAS. Individual products containing these compounds were not identified, highlighting a lack of transparency in product formulation disclosures. Continued use of PFAS in coating systems underscores the reliance on fluorinated chemistries and the need for an effective fluorine-free coating [9].

Due to their widespread occurrence, PFAS have become highly persistent pollutants in the environment and pose a threat to human health, as illustrated in figures 3-4 [7]. Regulatory agencies in the United States, Japan, and Europe have begun restricting these materials, prompting development of alternative coating technologies. Additionally, multiple lawsuits and enforcement actions have been filed against chemical and coating manufacturers for PFAS contamination, misleading environmental claims, and product-related exposure risks. These include litigation involving Dupont over PFAS water contamination settlements, PPG Industries over environmental contamination claims, 3M over Aqueous Film-Forming Foams (AFFF)-related PFAS liability claims, and other brother national litigation involving municipalities and individuals impacted by PFAS exposure [7a-d]. Although shorter-chain fluorocarbon alternatives have been introduced (e.g., C6 or C4 compounds), these materials display reduced bonding capability, rendering them ineffective [6-7].

Alternative non-fluorocarbon coating technologies have been explored to address the need for environmentally safe waterproofing systems. These approaches include silicone-based coatings, organic polymer-based systems, and conventional barrier coatings. Silicone-based coatings primarily serve as surface treatments, but moisture can penetrate over time [10]. Organic polymer-based coatings provide initial water resistance; however, they may display reduced durability under prolonged exposure, specifically in the presence of moisture. Epoxy and polyurethane-based coatings face similar limitations as they are highly sensitive to moisture in aqueous conditions [11]. Despite widespread commercial availability, many coating technologies are heavily reliant on incremental modifications of existing chemical formulations rather than developing new material systems. As a result, many current marketed products continue to face limitations with long-term durability under aggressive environmental conditions [10-11].

Among these approaches, sol-gel-based coatings display a promising solution. Unlike conventional coatings, sol-gel chemistry can form stable, three-dimensional inorganic-organic networks within the substrate material. However, large-scale manufacturing and reproducibility of sol-gel systems have remained challenging [12]. Despite these limitations, these networks can withstand abrasion, which enable improved long-term performance compared to traditional surface coatings [13]. These properties essentially eliminate the need for surface alteration, forming a dense, anti-corrosive protective layer that shields masonry from water intrusion. Sol-gel coatings remain attractive due to their low-temperature processing, and ability to form direct chemical bonds with surfaces, and ability to create durable hydrophobic barriers that reduce water intrusion and corrosion, while minimizing environmental impact [14].

Figure 5. *Field application of SCHN 158 on a masonry monument signage in First Colony HOA (Sugar Land, Texas).*

Figure 5 demonstrates the long-term durability of SCHN 158 under outdoor environmental exposure. The masonry monument previously experienced staining and environmental discoloration, attributed to surrounding vegetation. Prior to coating application,

the structure was cleaned using a low-pressure soft wash treatment (<1500 psi). Following application of SCHN 158, the masonry maintained its structural integrity and visual appearance for over seven years without requiring reapplication (bottom image). Without protective treatment, masonry structures exposed to prolonged moisture experience staining, cracking, delamination, and increased maintenance costs. Field implementation of SCHN 158 has covered more than 100 miles of masonry walls and to over 100 residential communities throughout the Houston area.

This study evaluates the performance of SCHN 158, a sol-gel-based hydrophobic nanocoating, in enhancing the durability of masonry. Performance was assessed through mass change analysis under aqueous exposure, acid corrosion testing, and sorptivity-based water absorption measurements. Sorptivity describes a material's ability to transport water through capillary action, serving as an important indicator of permeability and long-term durability. By comparing coated and uncoated samples, this study aims to assess SCHN158's capacity to reduce water transport, improve acid resistance, and enhance long-term structural stability.

Experimental

Sorptivity analysis provides an understanding of capillary-driven transport of water within porous materials such as concrete. Water transport follows diffusion-like behavior, where the rate of absorption is proportional to the square root of time, according to ASTM C1585 (Equation 1). The slope of the sorptivity curve demonstrates the rate at which water enters the pore structure, with steeper slopes indicating high levels of permeability and increased susceptibility to degradation [3,19-20].

Water absorption in porous materials, such as concrete, is governed by capillary-driven transport. According to ASTM C1585, cumulative water absorption (*I*), is proportional to the square root of time, shown in equation (1):

$$I = S_i \times t^{\frac{1}{2}} + b \qquad (1)$$

Where *I* represents cumulative water absorption, S_i represents sorptivity, *t* represents time, and *b* is a constant. Higher sorptivity indicates increased permeability and greater susceptibility to degradation due to the increased water transport through the material. The square root of time is used as water absorption increases over time in a diffusion-controlled manner.

a. Methods for Mass Analysis Experiment

Laboratory experiments were designed to approximate environmental conditions encountered in masonry infrastructure by exposing coated and uncoated masonry tiles to aqueous solutions representative of these environments.

Masonry tiles were used as the substrate material to evaluate the performance of protective coatings in preventing degradation in exposure to aqueous environments. Prior to coating, the samples were cut into uniform specimens to ensure consistent surface area and mass across all experimental samples. The surfaces of the tiles were then cleaned with acetone to remove surface contaminants, as they could interfere with coating adhesion. After cleaning, the samples were allowed to dry completely under ambient laboratory conditions. The initial mass of each specimen was measured using an analytical balance and recorded to establish a baseline for subsequent measurements following coating application and environmental exposure.

Three experimental groups were established to evaluate the effectiveness of different coating formulations. Each group consisted of three replicate tile specimens. The first group

served as the control and consisted of uncoated tiles. The second group was coated with a sol–gel formulation intended to act as a protective barrier against aqueous penetration and corrosive species. The third group consisted of tiles coated with a sol–gel formulation containing iodopropynyl butylcarbamate (IPBC), an antimicrobial additive. This was included in evaluating the potential effects of coating performance.

Coatings were uniformly applied to the tile surfaces using a controlled dipping method to ensure consistent coverage across all specimens. Following application, the coated tiles were either allowed to air-dry at room temperature or placed in a laboratory oven at low heat for approximately 30 minutes to facilitate solvent evaporation and initial curing. Although the coating becomes dry to the touch within one hour, continued diffusion into the substrate allows further crosslinking within the internal pore structure. This behavior differs from conventional film-forming coatings, which primarily remain on the material surface. After drying, the mass of each tile was measured again to determine the amount of coating deposited on the substrate.

To simulate environmental conditions relevant to industrial infrastructure, both coated and uncoated tiles were exposed to aqueous solutions including purified water and produced water. These solutions were selected to approximate the chemical conditions that masonry structures may encounter in subsurface environments associated with environmental exposure. Following the exposure period, the tiles were removed from the solutions, allowed to dry under ambient conditions, and weighed again using an analytical balance.

Mass measurements collected throughout the experiment were used to characterize coating performance. Each tile was weighed at the initial and final stages of the experiment: prior to experimentation and following 5-day environmental exposure. Differences between these measurements were used to determine coating uptake as well as changes in mass resulting from

exposure to aqueous environments. Percent mass change was calculated to facilitate comparison between coating formulations and exposure conditions. These measurements provided an indication of coating stability and the degree to which the coatings limited interaction between the masonry substrate and the surrounding environment. Experimental mass data obtained for the different coating formulations and exposure conditions were used to evaluate the relative effectiveness of the sol-gel based coatings.

b. Methods for Acid Corrosion Experiment

An additional experiment was conducted to test acid erosion on pristine and SCHN 158 Masonry-treated concrete blocks. The SCHN 158 concrete block was treated with SCHN 158 Masonry sealer by a foam roller and then dried/cured. Pristine and SCHN 158 concrete were dipped into a 1 Molar HCl or HNO_3 solution. Both solutions were highly acidic with a pH of 0. In intervals of 24 hours, both samples were retrieved from the acid and washed under running water. The blocks were then hand-brushed to remove any loose debris before weighing.

Results and Discussion

a. Results of Mass Analysis

Percent mass change relative to coated mass was calculated after water exposure to assess coating stability. Positive values indicate net mass gain due to potential water uptake or ion deposition, whereas negative values indicate material loss or possible coating degradation. The magnitude of percent change was used as an indicator of environmental stability under different ionic conditions.

Sol-gel-coated samples showed minimal mass loss across the exposure conditions. In dispenser water, the percent mass change ranged from 0% to 1.86%, with an average of 0.82%. In the samples soaked in purified water, the percentages ranged from -1% to 1.61%. In produced

water, the samples displayed greater variability as they ranged from -3.78 to 2.02%. Overall, sol-gel-coated samples showed minimal change across all water samples, indicating strong coating stability and resistance against water-induced mass transport.

The sol-gel coating mixed with IPBC additives displayed greater variability. In dispenser water, the percent mass ranged from -7.63 to 2.41%, with an average of -2.86%. In purified water, the mass percentage ranged from -0.45 to 1.36%, averaging 0.56%. In produced water samples, the percentages ranged from 0.68 to 1%. While purified and produced water samples remained stable, the variability in dispenser water samples suggests inconsistencies in coating application or additive dispersion. Despite this variability, both produced water and purified water samples indicate strong coating stability against aqueous exposure.

Overall, coatings that maintained percent of mass changes near zero demonstrated reduced interaction with water, which suggests improved barrier performance against moisture entry.

b. Results of Acid Corrosion Experiment

Figure 6. *SCHN 158-treated samples are represented by the left concrete block. Pristine (untreated) samples are represented by the right concrete block.*

The experiment compares SCHN 158 Masonry-treated concrete (left) and pristine (untreated) concrete (right). Both concrete blocks were immersed in 1 M HCl or HNO3 and photographed over time. This experiment simulated extreme acid exposure.

The pristine concrete samples exhibited progressive deterioration throughout the experiment. In initial stages, the pristine concrete showed surface roughening and material loss. As exposure continued, material loss, increased porosity, and loosening of aggregate particles were observed in the untreated sample. During advanced stage, pristine samples exhibited severe degradation, with the cement having lost its original shape, narrowing in the central region of the specimen, and collapsed along the edges. Severe surface corrosion and exposed aggregate particles were evident in the final images, indicating significant concrete degradation.

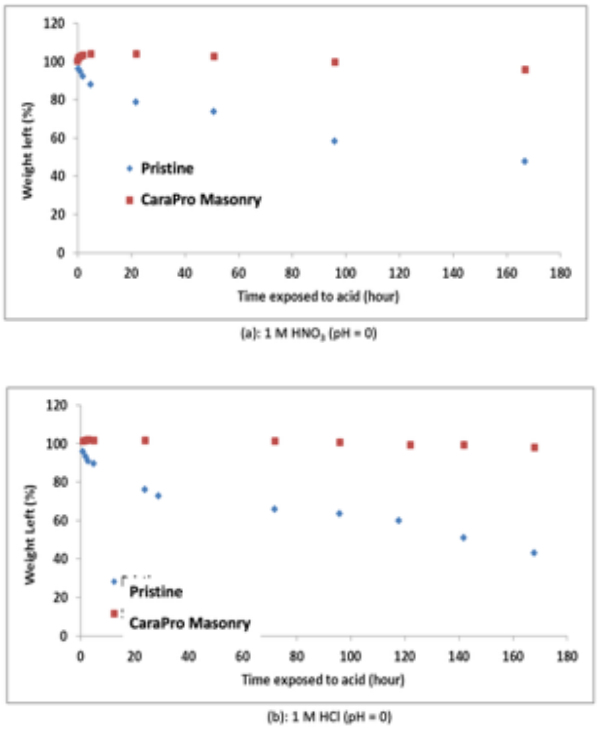

Figure 7. *Weight remaining (%) as a function of exposure time for pristine and SCHN 158 Masonry-treated concrete samples exposed to (a) 1 M HNO_3 and (b) 1 M HCl (pH = 0).*

In contrast, SCHN 158-treated samples maintained structural integrity throughout the exposure period. Minor visual changes were observed, and the treated sample maintained its original shape and surface texture throughout the experiment.

The pristine concrete samples exhibited a continuous decrease in weight with increasing exposure in both acid environments. In 1 molar nitric acid (Figure 7a), pristine samples showed a rapid initial weight decrease over the first 20 hours. The sample exhibits a final weight of nearly 45%, indicating 55% mass loss. The SCHN 158 samples, when tested against 1 molar nitric acid, retained approximately 100% of their mass with minimal variation throughout the experiment. Similarly, when testing pristine samples against 1 molar hydrochloric acid (Figure 7b), the samples showed a gradual decrease over time, with a final retained weight of 40%. In contrast, SCHN 158 samples remained near 100% of their original mass in both acid environments and further confirmed by visual observations.

These results show that untreated concrete is highly susceptible to acid-induced dissolution, whereas the sol-gel coating effectively limits acid entry and maintains structural integrity.

c. Water Absorption and Sorptivity Analysis

Change in absorption over time illustrates the rate and extent of water absorption in untreated and treated samples. The linear relationship between sorption and the square root of time confirms that water transport is governed by capillary-driven diffusion, with the slope of each curve corresponding to the material's sorptivity (Equation 1).

SCHN 158 consistently demonstrated the lowest sorption values at all time points compared to untreated and commercially coated samples. SCHN 158 exhibited the lowest slope and the slowest increase over time. These results indicate that SCHN 158 had the lowest water uptake rate and served as an effective barrier to capillary transport.

Water absorption behavior was measured using sorptivity analysis, where absorption (*I* or Cumulative infiltration) was plotted as a function of the square root of time (Equation 1).

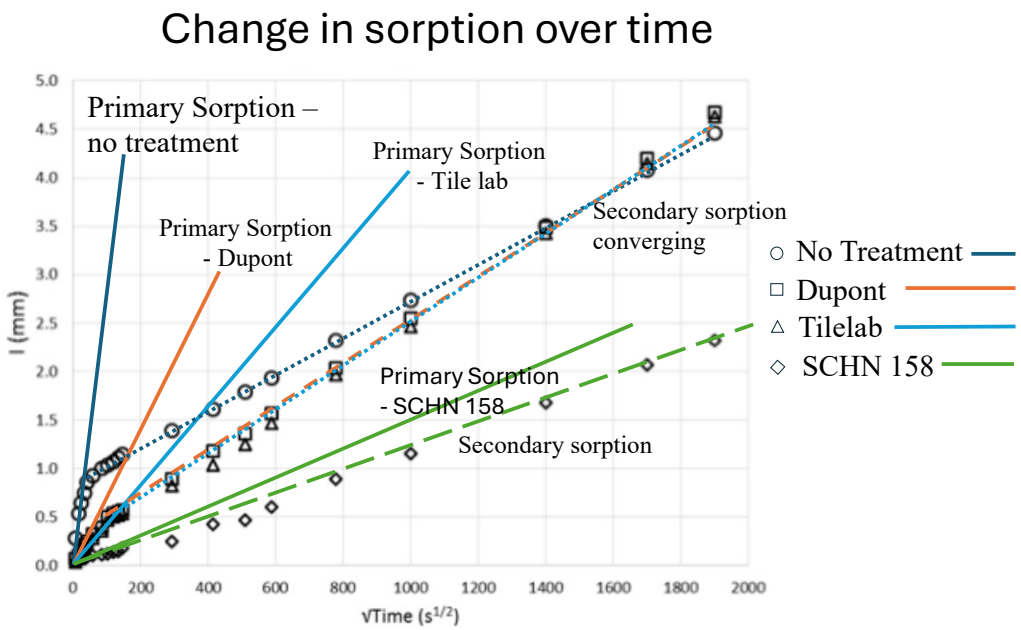

Figure 8. *Change in sorption (I) as a function of the square root of time for untreated and coated masonry samples.*

Change in absorption over time illustrates the rate and extent of water absorption in untreated and treated samples. The linear relationship between sorption and the square root of time confirms that water transport is governed by capillary-driven diffusion, with the slope of each curve corresponding to the material's sorptivity (Equation 1).

SCHN 158 consistently demonstrated the lowest sorption values at all time points compared to untreated and commercially coated samples. SCHN 158 exhibited the lowest slope and the slowest increase over time. These results indicate that SCHN 158 had the lowest water uptake rate and served as an effective barrier to capillary transport.

During the initial absorption phase, all samples exhibited high sorptivity due to rapid capillary uptake in unsaturated pores. As exposure time increased, absorption rates declined as pore saturation occurred, which resulted in a secondary sorption phase characterized by lower slopes. Untreated samples exhibited the highest sorption value across all time points, indicating rapid water uptake. Commercial coatings, such as DuPont and TileLab, exhibited intermediate

performance. These coatings displayed a reduced slope but were notably steep. Additionally, both DuPont and TileLab exhibited higher sorption values at $t^{1/2} = 900$ than the uncoated samples. This indicates a reduced long-term effectiveness of these coatings and suggests that they may lose barrier performance over time.

Initial sorption behavior was analyzed using early-time data collected over a six-hour period. During this phase, water uptake is primarily driven by capillary transport through unsaturated pore networks. While sorptivity provides insight into water penetration pathways, long-term adsorption behavior may also be influenced by adsorption interactions occurring within the masonry structure.

To further analyze this behavior, absorption processes were modeled using the Elovich equation, which is commonly used to describe systems where absorption rates decrease over time due to surface interactions and reduced availability of active sites **[15].** In this model, *a* and *b* are constants during the experimental process, while *t* denotes the absorption time. The constant a is regarded as the initial absorption rate because (dq_t/dt) approaches *a* when q_t approaches zero.

$$\frac{dq_t}{dt} = a \exp(-bq_t) \qquad (2)$$

For an adsorption system, let t_{ref} represent the longest operating time during absorption and q_{ref} represent the solid phase concentration at time $t = t_{ref}$. Thus, Eq. (2) can be rewritten as:

$$q_{ref} = \frac{1}{b} \ln(ab) + \frac{1}{b} \mathrm{Ln}(t_{ref}) \qquad (3)$$

Similarly, equation 3 can be rewritten as:

$$\frac{qt}{q_{ref}} = \frac{1}{q_{ref} b} \mathrm{Ln} \frac{t}{t_{ref}} + 1 \qquad (4)$$

Equation 5 represents a dimensionless Elovich model and can be used to evaluate equilibrium absorption behavior [15].

$$\frac{qt}{q_{ref}} = R_E \ln\left(\frac{t}{t_{ref}}\right) + 1 \quad (5)$$

These absorption models help evaluate whether water transport remains a reversible physical process or transitions toward irreversible material degradation. In untreated and commercially coated samples, prolonged exposure may promote leaching of core masonry constituents, such as mortar components and surface treatment materials. This degradation can contribute to delamination, brittleness, and increased structural vulnerability over time. In contrast, SCHN 158 exhibited a slower and more controlled increase in sorption values, suggesting that water uptake remains significantly reduced and potentially reversible. This behavior indicates improved long-term durability by its limitation of water ingress and reduction of structural degradation.

In real-world applications, prolonged water penetration accelerates masonry failure, exposes embedded steel reinforcement, and increases the risk of corrosion in infrastructure systems, including reinforced concrete structures, pipelines, and industrial facilities. The need for effective hydrophobic barriers is essential for improving long-term durability.

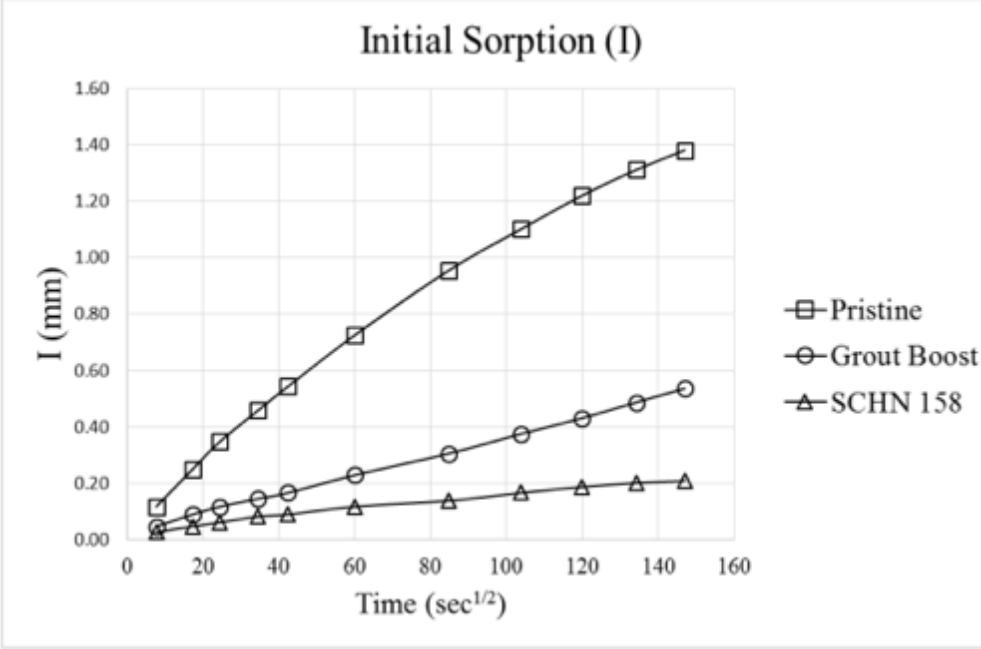

Figure 9. *Initial sorption (I) behavior over time ($t^{1/2}$) for pristine and coated samples during the early-stage water absorption (0-6 hours).*

Initial absorption was measured over a six-hour period, with time plotted on the x-axis and sorption (I) plotted on the y-axis. The relationship remained largely linear during early-stage absorption.

Pristine (untreated) samples exhibited the highest sorption values and the steepest slope, reaching approximately 1.38 mm at the highest time point. These results indicate rapid water uptake caused by high porosity and increased capillary transport pathways. Grout Boost samples exhibited lower sorption values, reaching approximately 0.54 mm at the highest time point, representing a 63% reduction relative to pristine samples. Although water absorption was reduced, the slope suggests that water penetration had still occurred over time.

SCHN 158 demonstrated the lowest sorption value, reaching approximately 0.20 mm, representing an 84% reduction compared to the pristine samples. The relatively low and controlled sorption behavior observed in SCHN 158-treated samples suggests that water transport occurs at a significantly lower rate due to reduced pore vacancies and fewer pathways for capillary transport.

These findings suggest that SCHN 158 may also have potential applications as an additive within masonry systems rather than solely as a surface coating. In practical applications, reduced water uptake helps limit grout degradation, microbial growth, and long-term structural degradation. Similar benefits may be applicable to industrial systems where water intrusion causes damage to pipelines, reinforced concrete, and other infrastructure.

Overall, both coatings reduced initial water absorption; however, SCHN 158 demonstrated the greatest reduction in both rate and extent of water uptake.

Secondary absorption was measured to assess the long-term behavior of coatings. The X-axis represents time, and the Y-axis represents sorption (*I*). As all lines increase with time, the relationship is linear.

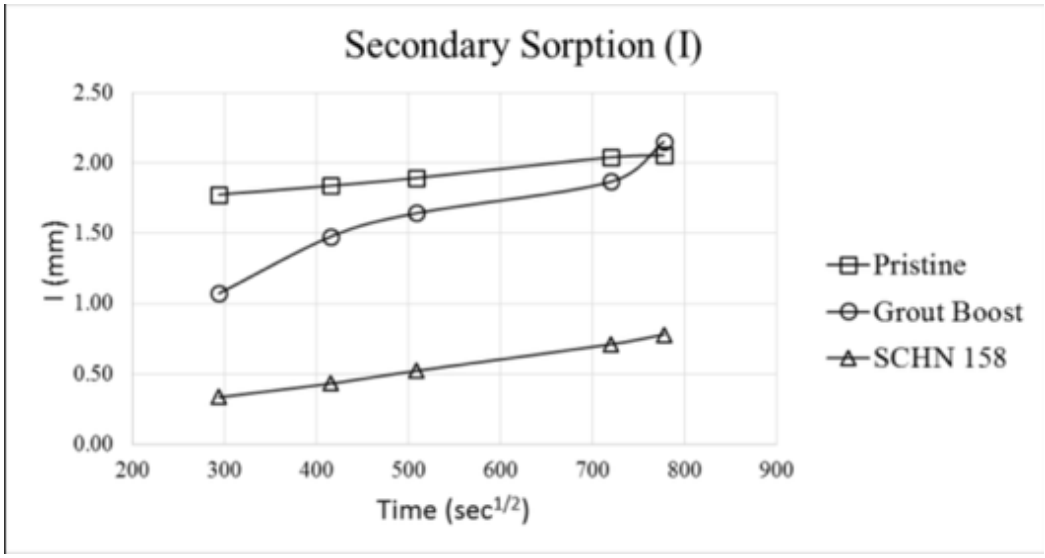

Figure 10. *Secondary sorption (I) behavior over time ($t^{1/2}$) for pristine and coated samples during prolonged exposure.*

Secondary sorption was measured to evaluate long-term coating performance. At this stage, pores of the samples are partially filled, and water continues to penetrate deeper into the sample. Pristine samples exhibited consistently high sorption values, increasing from approximately 1.8 mm to 2.0 mm. These results indicate high permeability of the samples. Grout Boost samples initially displayed lower sorption value (1.1 mm), indicating that the coating reduced

water uptake. However, sorption values rapidly increased at later time points ($t^{1/2}$ =800 sec), eventually exceeding untreated samples (2.1 mm). This suggests that the coating becomes less effective over time. In contrast, SCHN 158 samples maintained low sorption values throughout the duration, increasing from 0.38 mm to 0.57 mm. These results indicate that SCHN 158 effectively limits water absorption and transports over prolonged exposure. As water penetrates increasingly porous materials, essential cementitious components may gradually leach from the structure, accelerating the degradation process and reducing long-term durability. SCHN 158 appears to mitigate this process by maintaining lower permeability over prolonged exposure.

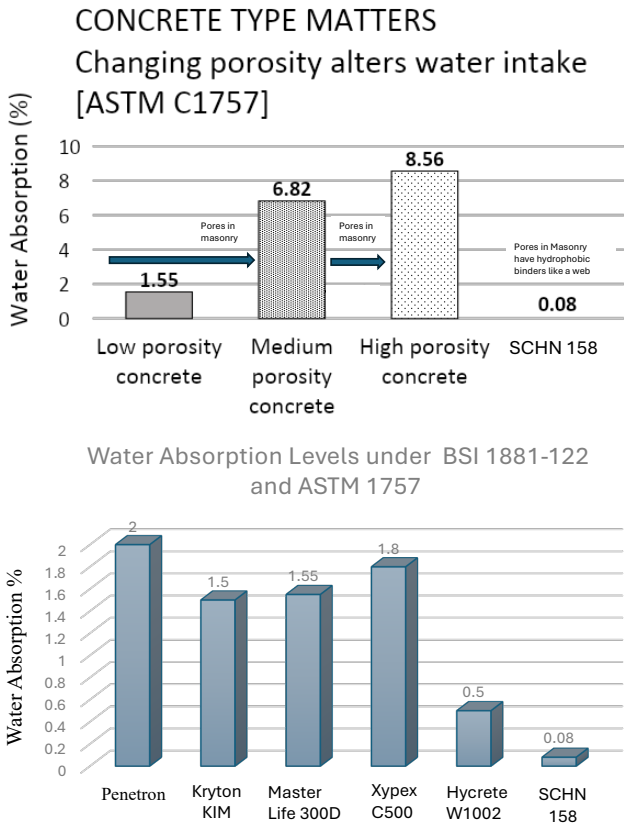

Figure 11. *Comparison of water absorption performance of SCHN 158 and commercially available waterproofing technologies under ASTM C1757 and BSI 1881-122 testing standards.*

Figure 11 compares SCHN 158 with other commercially available waterproofing technologies using ASTM C1757 water absorption testing. The samples were submerged in water and tested

once dry at approximately 30 minutes. SCHN 158 demonstrated the lowest water absorption value (0.08%) compared to Penetron (2.0%), Kryton KIM (1.95%), MasterLife 300D (1.55%), Xypex C500 (1.8%), and Hycrete W1002 (0.5%) [16]. These results further support the effectiveness of SCHN 158 in reducing water uptake compared with currently available technologies. The consequences of capillary-driven water transport extend beyond moisture absorption. Water transport supports the transport of aggressive species such as chlorides, sulfates, and acidic ions into masonry structures. These ions accelerate surface degradation, internal corrosion, and increased moisture vapor accumulation. These processes collectively contribute to the reduction of durability over time.

Discussion

The magnitude of mass change serves as an indicator of coating stability during aqueous exposure. Coatings that exhibited percent of changes near zero indicate minimal water uptake and reduced transport of dissolved species into the masonry substrate. SCHN 158 coated samples showed the least mass variation across different test environments. This low variation could be attributed to the structure of the sol-gel network, which limits interactions with aqueous environment [14, 17-18]. The sol-gel coating with IPBC additives displayed greater variability compared to the base sol-gel coating. The variability may be associated with inconsistencies with additive addition or coating uniformity.

The initial sorption graphs (Figure 9) represent the early stage of water uptake. The pristine (untreated) samples displayed the highest sorption values (1.38 mm) and the steepest slope, indicating rapid water ingress. The grout boost samples exhibited reduced water absorption to 0.54 mm, a 63% decrease compared to the pristine samples. The decreased values indicate that the coating partially blocks water entry. The SCHN 158 samples had the lowest value (0.20 mm),

representing an 85% reduction compared with pristine samples. The flatness of the slope, as seen in Figure. 9, indicates a strong reduction in sorptivity and higher resistance to initial water penetration.

Secondary sorption represents long-term water absorption (Figure 10). At this stage, water continues to penetrate deeper into the samples. The pristine samples had the highest sorption values (1.8-2.0 mm), indicating continued water uptake. Grout boost exhibited slightly higher sorption values than the pristine samples (2.1 mm). This reflects that the coating loses effectiveness over time, allowing increased water penetration. SCHN 158 samples displayed significantly lower values (0.75 mm), indicating consistent resistance to water absorption over prolonged exposure.

This behavior is characteristic of cementitious materials as the interconnected pore networks allow for the efficient transport of water into the bulk structure. The increased water ingress correlates to high permeability leading to transport of ions and acceleration of the degradation process [3,21]. Commercial coatings such as Grout Boost showed an initial decrease in sorptivity, indicating partial barrier effectiveness. However, the increase in sorptivity values over time indicates loss in the coating's effectiveness and increased water penetration. The prolonged exposure causes poor adhesion, microcracking, and gradual degradation of the coating layer [21]. The reduced performance of Grout Boost allows for the reinforcement of water transport pathways, leading to further reduced effectiveness.

The SCHN 158 sol-gel coating displayed consistently low sorptivity values in both initial and secondary absorption analysis (Figures 9-10). The reduction in slope and limited increase over time shows the coatings' effectiveness in restriction of capillary transport. The consistent performance of SCHN 158 can be attributed to Sol-gel's ability to form a three-dimensional

inorganic-organic network. The formation of the Silicon-Oxygen-Silicon linkages in the sol-gel process creates a difficult pathway for water entry and limits the extent of water absorption [22].

In terms of practicality, sorptivity is directly correlated with water movement in concrete, significantly impacting durability. Water transport carries dissolved substances such as toxic chemicals including PFAS, acids, salts, and ions. These substances are highly reactive with the cement matrix and cause significant structural weakening over time [3, 23]. The consequences of water transport play a significant role in the corrosion of embedded steel reinforcement. Penetration of water and dissolved substances (e.g., chlorides) can initiate corrosion reactions, accelerating degradation and crack formation (as seen in Figure 6). The formation of cracks further increases pressure and expansion within the reinforcement [23]. By reducing sorptivity, the rate of entry of aggressive ions and water is significantly reduced. In concrete systems, water ingress is identified as a significant driver of deterioration. By restricting fluid transport and reducing permeability, coatings such as SCHN 158 can extend the service life of infrastructure exposed to continuous moisture and aggressive chemicals [24].

The significant mass loss observed in pristine samples is consistent with the acid-induced degradation of cement material (Figure 7a-b). Material loss in the untreated samples occurred due to the reaction between the cement phases and the acid. A concrete structure is held together by cement phases ("glue"), such as calcium hydroxide and calcium silicate hydrate, which are highly alkaline and therefore react readily with acids. The reaction between alkaline compounds and acids produces soluble calcium salts, which leach out of the concrete. Progressive leaching of soluble calcium salts, such as $CaCl_2$ and $Ca(NO_3)_2$, leads to material loss. Critical damage occurs when calcium silicate hydrate undergoes decalcification, leading to structural degradation and decreased mechanical strength of the concrete. Research shows that calcium silicate hydrate is an essential hydration product in cement and is directly correlated with mechanical stability and strength [25].

As calcium is removed, increased pore enlargement and permeability occur [26]. As the concrete becomes more porous, the acid can diffuse deeper into the material, accelerating the reaction. Due to this cycle, the damage worsens over time [27].

Figure 12. *Chemical mechanism of acid attack on calcium hydroxide in cementitious materials. Acid reacts with alkaline cement phases to form soluble calcium salts, which leach from the structure and result in increased porosity and loss of structural integrity.*

In contrast, the SCHN 158-treated samples exhibited minimal mass loss, likely due to the coating's protective effect. The coating acts as a barrier between the concrete pores and the acid, limiting its diffusion. The primary focus of the coating is reducing acid penetration rather than solely chemical resistance. The coating inhibits the degradation cycle, thereby maintaining the structure and weight of the concrete. The visual degradation observed in Figure 6 aligns with the qualitative mass loss trends. The pristine samples exhibited highly visible surface erosion, aggregate exposure, and fragmentation. The SCHN 158 samples maintained their shape and appearance, indicating retention of material.

The consequences of acid corrosion are significant in real-world applications. In conventional infrastructure, acid penetration is a major driver of steel and iron reinforcement structure corrosion [23]. SCHN 158's ability to limit permeability allows for a reduction in corrosion and extends the service life of infrastructure that is exposed to harsh chemical environments, such as wastewater systems, pipelines, and other industrial facilities [23, 28]. Increased durability of concrete surfaces supports infrastructure longevity by minimizing corrosion-related structural stress. Increased alkalinity of masonry corrosion deteriorates steel and iron reinforcing bars, affecting structural integrity.

Figure 13. *a) heavy, reinforced concrete column, seen before and after the concrete has been cast in place around its rebar frame. Photos: Benutzer:Störfix. Combination: Florian.Arnd, CC BY-SA 3.0 <http://creativecommons.org/licenses/by-sa/3.0/>, via Wikimedia Commons, b) Structure of reinforced concrete pipe showing the concrete wall, inner lining, and embedded steel reinforcement susceptible to corrosion.*

The materials of reinforced concrete pipes, specifically porous concrete and internal rebar, are uniquely vulnerable to constant water saturation. With this exposure, industrial infrastructure fails to maintain deep-matrix integrity. Integrating SCHN 158 into these systems moves infrastructure protection beyond evasive coverage. This high-density nanocoating creates a durable network that reinforces industrial infrastructure at the molecular level. By sealing the pores in masonry and fusing with rebar material, SCHN 158 provides an effective shield that protects reinforced concrete structures against water infiltration. This approach ensures that infrastructure remains structurally sound and resilient against adverse environmental conditions.

These findings are significant in the context of replacing fluorine-based coatings, specifically those derived from PFAS chemistries. These compounds are widely used because of their hydrophobicity and chemical stability, which are attributed to their amphiphilic molecular structure and carbon-fluorine bond, respectively. However, their high stability is also attributed to high persistence in various environmental media, including air, water, and soil, ultimately impacting the environment and human health [6-7, 29].

A critical aspect of PFAS environmental impact is their mobility in aqueous environments. PFAS can be distributed through groundwater, streams and oceans, and the atmosphere, leading to widespread contamination beyond the source. Research indicates that their partitioning behavior is strongly influenced by the length of their perfluorinated chain and the identity of their terminal group. Short-chain PFAS remain dissolved in aqueous environments due to their high hydrophilicity [29, 30]. As a result, PFAS contamination is closely correlated with water transport pathways, a primary mechanism for environmental and biological contamination, as seen in Figure 3.

In protective coatings for masonry and concrete, water transport is a primary pathway for the entry of corrosive species, such as chlorides, hydrogen ions, and other dissolved substances. This pathway allows these species to penetrate the material and reach the iron reinforcement, leading to structural degradation, cracking, and ultimately material failure. Thus, controlling water movement is essential for reducing both environmental exposure and internal corrosion in infrastructure [22,31,32].

Results of this study indicate that SCHN 158 coating reduces water movement and entry of corrosive species, as evidenced by low sorptivity values and minimal mass changes. This barrier effect plays an essential role in protecting steel reinforcement from corrosion, addressing a significant mechanism of long-term infrastructure degradation. Rather than using fluorinated chemistry, SCHN 158 forms a stable sol-gel network that acts as an effective barrier to water and other substances that cause corrosion. These results show that SCHN 158 effectively reduces corrosion while mitigating environmental and health risks associated with PFAS materials [33].

Conclusion

This study evaluated the effectiveness of this sol-gel-based coating (SCHN 158) in improving the durability of masonry materials in acidic and aqueous conditions. The results show that SCHN 158 significantly reduced water transport, as evidenced by its low sorptivity values and by comparisons with commercial coated and untreated samples. Additionally, SCHN 158 displayed minimal mass variation and superior resistance to acid-induced degradation. SCHN 158 provides a transformative approach to industrial corrosion through the ability to limit water ingress, thereby halting the entry of corrosive agents. By establishing a molecular barrier through sealing the capillary networks of the surrounding masonry, SCHN 158 effectively neutralizes water transport.

Beyond mechanical performance, this study acknowledges SCHN 158 as an environmentally benign alternative to the PFAS family. As pressure increases to regulate the use of persistent fluorinated chemicals, the development of fluorine-free, high-performing barriers becomes both industrially and environmentally imperative. Ultimately, the implementation of SCHN 158 represents a pivotal advancement in material science, offering an expansive solution to industrial corrosion. The ability to extend the service life of reinforced masonry and rebar structures while reducing the maintenance and safety risks associated with internal corrosion and masonry failure creates a new standard for the next generation of durable, eco-conscious infrastructure.

References:

[1] Capital Masonry. The Importance of Waterproofing Masonry. n.d. https://www.capmasonry.com/the-importance-of-waterproofing-in-masonry

[2] Advanced FRP Systems. Internal Pipe Corrosion: Causes and Solutions. **2022**. https://www.advancedfrpsystems.com/internal-pipe-corrosion/

[3] Yoo, J.-H.; Lee, H.-S.; Ismail, M. A. An Analytical Study on the Water Penetration and Diffusion into Concrete under Water Pressure. *Construction and Building Materials* **2011**, *25* (1), 99–108. https://doi.org/10.1016/j.conbuildmat.2010.06.052

[4] Maraşlı, M.; Subaşı, S.; Ramazanoğlu, D.; Özdal, V.; Hatipoglu, Y. Water Penetration Effects on Concrete Strength and Prevention Approaches. **2023**.

[5] Koch, G. H.; Varney, J.; Thompson, N.; Moghissi, O.; Gould, M.; Payer, J. International Measures of Prevention, Application, and Economics of Corrosion Technologies Study. NACE International, **2016**. http://impact.nace.org/documents/ccsupp.pdf

[6] Pizzorno, J. Fluorocarbons (PFAS)—The Forever Chemicals. *Integrative Medicine (Encinitas)* **2023**, *22* (6), 6–10. PMID: 38404606.

[7] Panieri, E.; Baralic, K.; Djukic-Cosic, D.; Buha Djordjevic, A.; Saso, L. PFAS Molecules: A Major Concern for the Human Health and the Environment. *Toxics* **2022**, *10* (2), 44. https://doi.org/10.3390/toxics10020044

[7a] Environment Litigation Group. Court Approves Massive $1.1 Billion Settlement with DuPont to Resolve Forever Chemicals Contamination Suits. n.d. https://www.environmentallitigationgroup.com/news/court-approves-massive-1-1-billion-settlement-with-dupont-to-resolve-forever-chemicals-contamination-suits/

[7b] PennEnvironment and Sierra Club v. PPG Industries, Inc., Civil Action No. 12-342 (W.D. Pa. **2024**). United States District Court for the Western District of Pennsylvania. https://www.tpmlaw.com/pennenvironment-v-ppg-industries

[7c] Keller Rohrback L.L.P. AFFF PFAS Liability Litigation. n.d. https://www.kellerrohrback.com/currentcases/afff-pfas-liability-litigation

[7d] Consumer Notice. PFAS Lawsuit Overview. n.d. https://www.consumernotice.org/legal/pfas-lawsuit/

[8] U.S. Environmental Protection Agency. Our Current Understanding of the Human Health and Environmental Risks of PFAS. n.d. https://www.epa.gov/pfas/our-current-understanding-human-health-and-environmental-risks-pfas (accessed April 24, 2026).

[9] Ehrlich, B. PFAS Found in Paint but Not on the Ingredient List. *Building Green*, **2023**. https://www.buildinggreen.com/newsbrief/pfas-found-paint-not-ingredient-list

[10] Hu, P.; Xie, Q.; Ma, C.; Zhang, G. Silicone-Based Fouling-Release Coatings for Marine Antifouling. *Langmuir* **2020**, *36* (9), 2170–2183. https://doi.org/10.1021/acs.langmuir.9b03926

[11] Xia, L.; Gui, T.; Wang, J.; Tian, H.; Wang, Y.; Ning, L.; Wu, L. Bio-Based Coatings: Progress, Challenges and Future Perspectives. *Polymers* **2025**, *17* (24), 3266. https://doi.org/10.3390/polym17243266

[12] Integricote, collaboration documents, **2012**.

[13] Minkiewicz, J.; Jones, G. M.; Ghanizadeh, S.; Bostanchi, S.; Wasely, T. J.; Aminorraya Yamini, S.; Nekouie, V. Large-Scale Manufacturing of Solid-State Electrolytes: Challenges, Progress, and Prospects. *Open Ceramics* **2023**, *16*, 100497.

[14] Kate, R. S.; Khalate, S. A.; Deokate, R. J. Overview of Nanostructured Metal Oxides and Pure Nickel Oxide (NiO) Electrodes for Supercapacitors: A Review. *Journal of Alloys and Compounds* **2018**, *734*, 89–111. https://doi.org/10.1016/j.jallcom.2017.10.262

[15] Wu, F.-C.; Tseng, R.-L.; Juang, R.-S. Characteristics of Elovich Equation Used for the Analysis of Adsorption Kinetics in Dye-Chitosan Systems. *Chemical Engineering Journal* **2009**, *150* (2–3), 366.

[16] Hycrete Inc. Hycrete Testing Summary. Hycrete, Inc., **2023**. https://hycrete.com/wp-content/uploads/2023/02/Hycrete-Testing-Summary-JAN23.pdf

[17] Biswas, A.; Friend, C. S.; Prasad, P. N. Ceramic Nanocomposites with Organic Phases, Optics. *Encyclopedia of Materials: Science and Technology* **2001**, 1072–1080. https://doi.org/10.1016/b0-08-043152-6/00198-4

[18] Wu, Y.; Li, M.; Wahyudi, W.; Sheng, G.; Miao, X.; Anthopoulos, T. D.; Huang, K.-W.; Li, Y.; Lai, Z. Performance and Stability Improvement of Layered NCM Lithium-Ion Batteries at High Voltage by a Microporous Al_2O_3 Sol–Gel Coating. *ACS Omega* **2019**, *4* (9), 13972–13980. https://doi.org/10.1021/acsomega.9b01706

[19] ASTM C1585-20. Standard Test Method for Measurement of Rate of Absorption of Water by Hydraulic-Cement Concretes. ASTM International, West Conshohocken, PA, **2020**. https://store.astm.org/c1585-20.html

[20] Amran, Y. H. M.; Farzadnia, N.; Abang Ali, A. A. Properties and Applications of Foamed Concrete; a Review. *Construction and Building Materials* **2015**, *101*, 990–1005. https://doi.org/10.1016/j.conbuildmat.2015.10.112

[21] Mahi, M. S. H.; Ridoy, T. A.; Sarder, A. A. Corrosion Mechanisms in Reinforced Concrete: Causes, Effects, and Sustainable Mitigation Strategies. *Current Problems in Research* **2025**, *1* (1), 52–66. https://doi.org/10.70028/cpir.v1i1.27

[22] Understanding Sol-Gel Coatings: A New Innovation in Surface Protection. Premera Coatings UAE, **2024**. https://premeracoatings.ae/understanding-sol-gel-coatings-a-new-innovation-in-surface-protection/

[23] Mahmoodian, M. *Reliability and Maintainability of In-Service Pipelines*. Gulf Professional Publishing: Oxford, **2018**; Chapter 1.

[24] Mori, T.; Nonaka, T.; Tazaki, K.; Koga, M.; Hikosaka, Y.; Noda, S. Interactions of Nutrients, Moisture and pH on Microbial Corrosion of Concrete Sewer Pipes. *Water Research* **1992**, *26* (1). https://doi.org/10.1016/0043-1354(92)90107-F

[25] Liu, X.; Feng, P.; Yu, X.; Huang, J. Decalcification of Calcium Silicate Hydrate (C-S-H) under Aggressive Solution Attack. *Construction and Building Materials* **2022**, *342*, 127988. https://doi.org/10.1016/j.conbuildmat.2022.127988

[26] Zhang, W.; Zhang, B.; Sun, J.; Dang, J.; Guo, X.; Li, K.; Huang, B.-T.; Dong, B.; Ma, H.; Hou, D. Insight into the Decalcification Mechanism of Calcium Silicate Hydrate under a Water–Heat–Salt Environment. *ACS Sustainable Chemistry & Engineering* **2025**, *14* (1), 483–496. https://doi.org/10.1021/acssuschemeng.5c10232

[27] Li, B.; Yang, H.; Yuan, X. Durability of Concrete Subjected to Acidic Exposure under Flexural Loading. *Advances in Cement Research* **2024**, *36* (10), 508–516. https://doi.org/10.1680/jadcr.23.00101

[28] Qiu, L.; Dong, S.; Ashour, A.; Han, B. Antimicrobial Concrete for Smart and Durable Infrastructures: A Review. *Construction and Building Materials* **2020**, *260*, 120456. https://doi.org/10.1016/j.conbuildmat.2020.120456

[29] Buck, R. C.; Franklin, J.; Berger, U.; Conder, J. M.; Cousins, I. T.; de Voogt, P.; Jensen, A. A.; Kannan, K.; Mabury, S. A.; van Leeuwen, S. P. Perfluoroalkyl and Polyfluoroalkyl Substances in the Environment: Terminology, Classification, and Origins. *Integrated Environmental Assessment and Management* **2011**, *7* (4), 513–541. https://doi.org/10.1002/ieam.258

[30] Shaffer, K. W.; Lee, C.-S.; Ye, X.; Graffam, M.; Paulsen, R. J.; McDonough, C. A.; Venkatesan, A. K.; Gobler, C. J. Fate and Transport of Per- and Polyfluoroalkyl Substances (PFAS) across the Groundwater-to-Estuary Continuum in an Aqueous Film Forming Foam (AFFF)-Impacted Watershed. *Environmental Pollution* **2026**, *390*, 127486. https://doi.org/10.1016/j.envpol.2025.127486

[31] Dragovic, H.; Damaceno, D. S.; Meyer, O. H. H.; Ervik, Å. Water Transport and Corrosion under Insulation: Experimental Investigations of Drying in Mineral Wool. *Process Safety*

and Environmental Protection **2024**, *190*, 198–210. https://doi.org/10.1016/j.psep.2024.08.016

[32] Kim, Y.-J.; Bahn, C. B.; Baek, S. H.; Choi, W.; Song, G. D. Crevice Chemistry and Corrosion in High Temperature Water: A Review. *Nuclear Engineering and Technology* **2024**, *56* (8), 3112–3122. https://doi.org/10.1016/j.net.2024.03.010

[33] Wen, J.; Wilkes, G. L. Organic/Inorganic Hybrid Network Materials by the Sol−Gel Approach. *Chemistry of Materials* **1996**, *8* (8), 1667–1681. https://doi.org/10.1021/cm9601143